JOC The Journal of Organic Chemistry

Article

pubs.acs.org/joc

Diastereodifferentiating Photocyclodimerization of 2-Anthracenecarboxylates Tethered to a Cyclic Tetrasaccharide Scaffold: Critical Control of Photoreactivity and Stereoselectivity

Gaku Fukuhara,*[,†] Tomohiro Nakamura,[†] Yuko Kawanami,[†] Cheng Yang,[†] Tadashi Mori,[†] Hiroyuki Hiramatsu,[‡] Yasufumi Dan-oh,[‡] Tomoyuki Nishimoto,[‡] Kazuo Tsujimoto,[‡] and Yoshihisa Inoue*[,†]

[†]Department of Applied Chemistry, Osaka University, 2-1 Yamada-oka, Suita 565-0871, Japan

[‡]Hayashibara Co., Ltd., 1-1-3 Shimoishii, Kita-ku, Okayama 700-0907, Japan

Supporting Information

ABSTRACT: From a complex mixture of mono- and di-2-anthracenecarboxylic acid (AC) esters of cyclic nigerosylnigerose (CNN), two monoesters (2^B and 6^A) and four diesters in which AC was introduced on the transannular B/D (2^B2^D), adjacent A/B and A/D (6^A2^B and 6^A2^D), and same B/B (2^B3^B) nigerose rings were isolated. Possessing two ACs at distant positions, 2^B2^D and 6^A2^D showed negative Cotton effects for the ^1B_b band, the intensities of which were stronger than that of 6^A. 2^B2^D and 6^A2^D slowly photocyclodimerized to give HH dimers **3*** and **4** with 57% and 81% HH selectivity, respectively, which were appreciably higher than that for 6^A (34%), while the enantiomeric excesses (ee's) of *anti*-HH dimer **3*** were 2% and −18%, respectively. In contrast, 6^A2^B and 2^B3^B carrying two ACs on adjacent A and B rings or at vicinal positions on the B ring, respectively, exhibited strong positive CD couplets, the amplitudes of which amounted to 97 and 409 M^{-1} cm^{-1}, respectively. Upon irradiation, 6^A2^B afforded **3*** with −62% ee and **4** in 96% combined yield, whereas 2^B3^B gave almost exclusively **3*** with −99% ee in 96% yield, likely as a result of the introduction of two ACs at the vicinal positions of the rigid CNN scaffold.

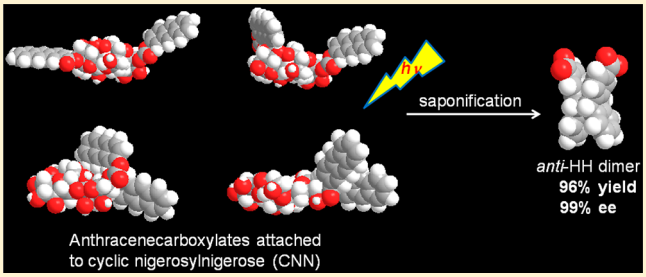

INTRODUCTION

Photochirogenesis has become more popular in recent years as a method for preparing optically active compounds through electronically excited states. A variety of strategies have hitherto been proposed and examined for efficient enantio- and diastereodifferentiation in various chiral photochemical reactions.[1] Nevertheless, simultaneously achieving high chemical and optical yields still remains a challenge in current photochemistry. This is due to the lack of reliable tools and incomplete knowledge about the factors and mechanisms for controlling the enantio- or diastereotopic face selectivity of the photosubstrate in the ground and excited states. For this purpose, a wide range of chiral auxiliaries and scaffolds have been used to afford moderate to high diastereomeric excesses (de's) for several diastereodifferentiating photoreactions, including photocyclization of diarylethenes (28−100% de),[2] photoisomerization of cyclooctene (21−43% de),[3] [2 + 2] photocyclodimerization of cinnamates (46−97% de),[4] photocycloadditions of enones to olefins (56−91% de),[5] and the Paternò−Büchi reaction of ketones with olefins (7−97%),[6] although the chemical yields reported for these reactions are not very high (55−99%).

Diastereodifferentiating [4 + 4] photocyclodimerizations of 2-anthracenecarboxylates (ACs) (Scheme 1) tethered to cellulose,[7a] amylose,[7b] and α-cyclodextrin (CDx)[7c] scaffolds have also been examined and were found to afford *anti*-head-to-head (*anti*-HH) cyclodimer **3*** in 5−22%, 1−10%, and 8−90% de, respectively, in good chemical yields of up to 81%.[7c] These results appeared to indicate that tethering two ACs to a chiral scaffold is a promising strategy but not sufficient to achieve the ultimate chemical and optical yields. Hence, we proposed the "dual supramolecular" approach using α-CDx as a chiral scaffold and γ-CDx as a confining host, which worked extremely well indeed in controlling both the ground-state conformation and the subsequent photocyclodimerization of two ACs on an α-CDx scaffold to afford **3*** with 99% enantiomeric excess (ee) in 98% yield.[7c] This result unequivocally revealed that reducing the conformational freedom is another effective tool for enhancing the stereoselectivity of the photocyclodimerization.

Cyclic nigerosylnigerose (CNN), *cyclo*-{→6)-α-D-Glc*p*-(1→3)-α-D-Glc*p*-(1→6)-α-D-Glc*p*-(1→3)-α-D-Glc*p*-(1→}, [8] is a relatively recently reported cyclic tetrasaccharide that is produced from alternan, a sort of dextran, by *Bacillus* sp. NRRL B-21195 strain and also from starch by *Bacillus globisporus* C11 and N75 strains and *Arthrobacter globiformis* A19 strain. X-ray crystallo-

Received: September 6, 2013
Published: October 4, 2013

   dx.doi.org/10.1021/jo401977f | J. Org. Chem. 2013, 78, 10996−11006

Scheme 1. Diastereodifferentiating Photocyclodimerization of 2-Anthracenecarboxylate (AC) Tethered to a Chiral Scaffold (R*)

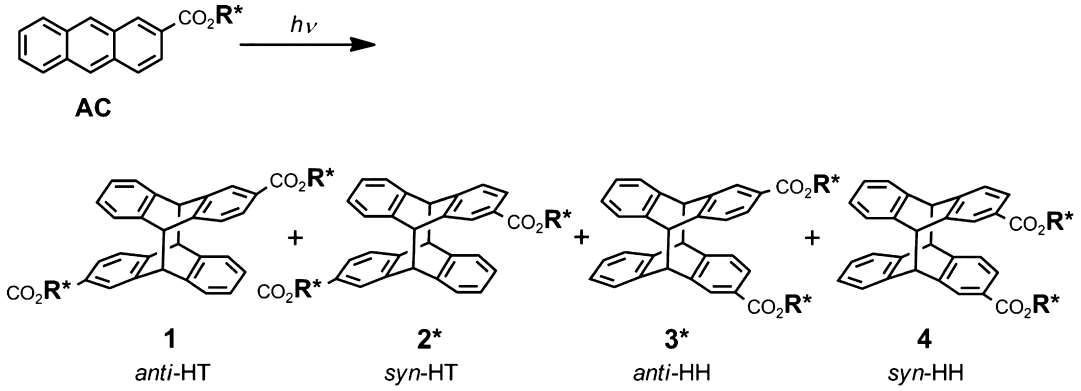

Chart 1. Structures of CNN[8b] and $2^B,3^B$-Di-2-anthroyl-CNN (2^B3^B)

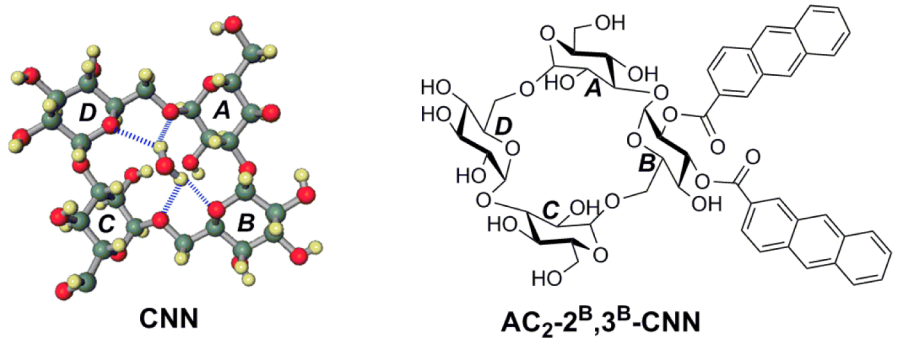

graphic studies revealed the inherently rigid skeleton of CNN, which is reinforced by a transannular hydrogen bond bridging the A and C nigerose units and also by a water molecule sitting in the center of the ring to fix all of the nigerose units with four hydrogen bonds, which remain intact even in DMSO and can be detected by NMR (Chart 1).[8b] For this reason, the CNN skeleton was expected to serve as a conformationally robust chiral scaffold for AC photocyclodimerization. In reality, selective esterification of the primary hydroxyl group in each nigerose ring turned out to be practically infeasible after several attempts under a variety of esterification conditions. Thus, the primary and secondary hydroxyls of CNN were almost randomly esterified to give a complex mixture of mono- and dianthryl esters, from which $2^B,3^B$-di-2-anthroyl-CNN (2^B3^B) was isolated by HPLC and subjected to photoirradiation to somewhat luckily achieve the nearly ultimate stereocontrol, affording essentially enantiopure **3** as the sole product (99% ee and 96% yield).[9]

The photochirogenesis result obtained for 2^B3^B was certainly satisfactory, but we did not fully understand why and how such excellent stereocontrol was achievable in this photochirogenic system. In the present study, we isolated some of the important mono- and dianthroyl derivatives of CNN by careful HPLC and comparatively studied the chiroptical properties and the photophysical and photochemical behaviors of these regioisomeric AC- and AC_2-CNN esters. The comparative studies will provide us with deeper mechanistic insights into the factors that control the stereochemical outcomes of this diastereodifferentiating photocyclodimerization of AC on the CNN scaffold.

RESULTS AND DISCUSSION

Synthesis, Isolation, and Characterization of AC- and AC_2-CNNs. For better selectivity and yield upon esterification, three typical esterification conditions for saccharides were examined, as no standard procedures had been established for CNN. First, AC chloride (4 equiv) was reacted with CNN in dry pyridine, and after workup, the product mixture was subjected to MALDI-TOF MS analysis to show multiple peaks assignable to AC- and AC_2-CNNs, but the relative intensities of the diester peaks were smaller than those of the monoester peaks. Then the esterification of CNN with AC (6 equiv) was performed in dry DMF by using *N*,*N*′-dicyclohexylcarbodiimide (DCC) and 1-hydroxybenzotriazole (HOBt). MS and NMR analysis of the product mixture showed only small peaks for the mono- and diesters. Hence, CNN was esterified with AC (3 equiv) in dry DMF using DCC and 4-(*N*,*N*-dimethylamino)-pyridine (DMAP) to give a mixture of mono-, di-, and (in small amounts) triesters, as identified by MS analysis [see the Supporting Information (SI) for details].

The crude precipitate obtained by pouring the filtered reaction mixture into diethyl ether was added to a 1:3 mixture of CH_3CN and H_2O, and the resulting suspension was ultrasonicated for 1 h and filtered to remove the insoluble residues. The filtrate thus obtained was subjected to analytical HPLC on a Cosmosil $5C_{18}$-AR-II column eluted by 25:75 CH_3CN/H_2O to give the chromatogram shown in Figure 1, which indicates that the esterification is not very regioselective, showing five peaks of varying intensities in the monoester region. MALDI-TOF MS analyses of the four major fractions 1−4 in Figure 1 unequivocally revealed that these are regioisomeric AC monoesters of CNN. This mixture was

dx.doi.org/10.1021/jo401977f | J. Org. Chem. 2013, 78, 10996−11006

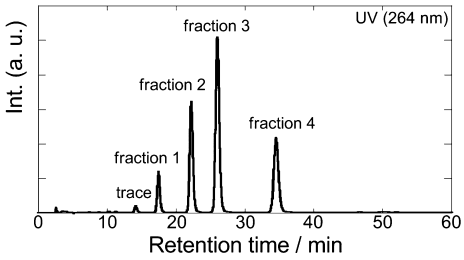

Figure 1. HPLC chromatogram (UV monitoring at 264 nm) of the monoesters extracted into a 1:3 CH_3CN/H_2O mixture by ultrasonication from the crude precipitate obtained by the esterification of CNN by AC with DCC/DMAP.

subjected to preparative HPLC on a Sumipax ODS eluted with 23:77 CH_3CN/H_2O (see Figure S2 in the SI). Fractions 2 and 3 were collected in large enough quantities for various 1D and 2D NMR spectral analyses (see Figures S3−S6 in the SI), which enabled us to assign fraction 2 as 2^B-(2-anthroyl)-CNN (**2^B**) and fraction 3 as 6^A-(2-anthroyl)-CNN (**6^A**) (Chart 2), while the fractions 1 and 4 were isolated in smaller amounts that were not enough for full NMR assignments to be made.

Since the diesters (AC_2-CNNs) were not soluble in 1:3 CH_3CN/H_2O, the crude precipitate mentioned above was dispersed in more hydrophobic 45:55 CH_3CN/H_2O, sonicated for 1 h, and then filtered. The clear filtrate obtained was subjected to HPLC analysis on the same column eluted with 45:55 CH_3CN/H_2O, which gave the chromatogram shown in Figure 2. The chromatogram monitored by UV (Figure 2a) revealed the monoester peaks at retention times of <5 min and also the overlapping diester peaks spread over the retention times 8−32 min. This complexity seems reasonable, since at least four regioisomeric AC-CNNs out of the six possible ones were produced upon monoesterification and the second esterification should also be similarly nonselective. However, such randomness upon esterification of the primary and secondary hydroxyls in CNN was not readily anticipated from the very selective esterification of the primary hydroxyl group at the 6-position of CDx,[10] for which the reduced reactivity of the secondary hydroxyls due to the hydrogen-bonding network around the secondary rim of CDx is likely to be responsible.

In the previous study,[9] we isolated from the complex mixture only the last-eluted diester, **2^B3^B** (Figure 2). In the present study, we wanted to retrieve not only intramolecularly photodimerizable but also photoinert diesters to obtain a better understanding of the factors that control the rate and diastereoselectivity of the photocyclodimerization of ACs introduced at different positions of the CNN scaffold. Obviously, our choice was not totally free but subject to the HPLC resolution.

In choosing the "right" diesters to be picked up from the mixture, HPLC with a tandem UV−fluorescence monitoring system was extremely useful. Figure 2a illustrates the HPLC trace of the AC- and AC_2-CNN mixture detected by UV at 264 nm, onto which the HPLC trace detected by fluorescence at 420 nm (with excitation at 254 nm) is superimposed in red in Figure 2b; the intensities were normalized to the highest monoester peak at 4 min. Although most of the mono- and diester peaks were comparable in intensity in the two traces, some of the diesters (eluted at ca. 15, 17, 19, and 32 min) showed much smaller intensities upon fluorescence detection. This was due to the relatively strong excitation light at 254 nm used in the fluorescence detector, which caused the intramolecular photocyclodimerization of sterically allowed AC_2-CNNs with an accompanying decrease in the AC fluorescence monitored at 420 nm. This contrasting behavior of reactive and unreactive AC_2-CNNs enabled us to choose the desired diesters. Fortunately, most of the reactive diesters were baseline-separated upon chiral HPLC (Figure 2), except for the one eluted at 19 min. We therefore isolated the photochemically inert fraction A and the photoreactive fractions B and C, as well as **2^B3^B** as reported earlier,[9] by preparative HPLC on a Sumipax ODS eluted with 42:58 CH_3CN/H_2O (see Figure S7 in the SI). 1D and 2D NMR spectral analyses (Figures S8−S13 in the SI) enabled us to assign fraction A as 2^B,2^D-di-2-anthroyl-CNN (**2^B2^D**), fraction B as 6^A,2^D-di-2-anthroyl-CNN (**6^A2^D**), and fraction C as 6^A,2^B-di-2-anthroyl-CNN (**6^A2^B**) (see Chart 3).

Although the isolated fractions account for only two-fifths of the total diester fractions detected in the UV-monitored chromatogram, we can briefly discuss the relative reactivities of the six independent hydroxyl groups of CNN from the product distribution of **2^B2^D**, **6^A2^D**, **6^A2^B**, and **2^B3^B** isolated in this study (Table 1). It seems crucial that only the 2^B- and 2^D- (which are equivalent unless further substitution occurs), 3^B-, and 6^A-hydroxyls were esterified, while the 2^A-, 4^A-, and 4^B-hydroxyls remained intact (as far as the isolated mono- and diesters are concerned). The inertness of the 2^A-hydroxyl may be rationalized by the intramolecular hydrogen-bonding interaction with the 2^C-hydroxyl observed at least in the crystal,[8b] but the inertness of the 4^A- and 4^B-hydroxyls cannot be immediately rationalized. Nevertheless, the product distribution listed in Table 1 is intriguing, reflecting the relative reactivity of

Chart 2. Structures of 2^B-(2-Anthroyl)-CNN (2^B) and 6^A-(2-Anthroyl)-CNN (6^A)

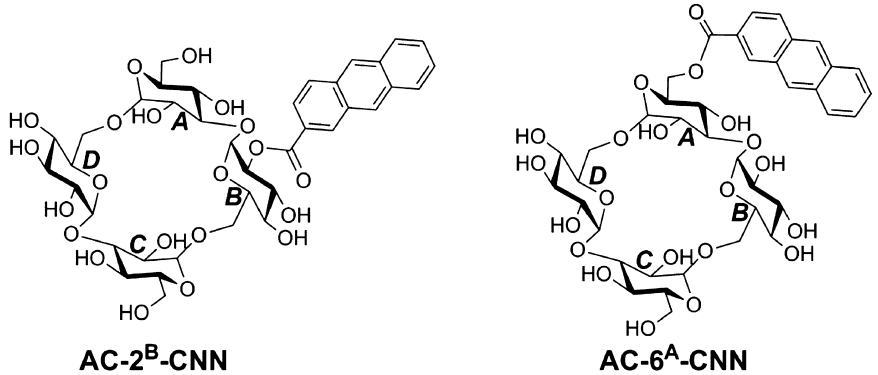

dx.doi.org/10.1021/jo401977f | J. Org. Chem. 2013, 78, 10996−11006

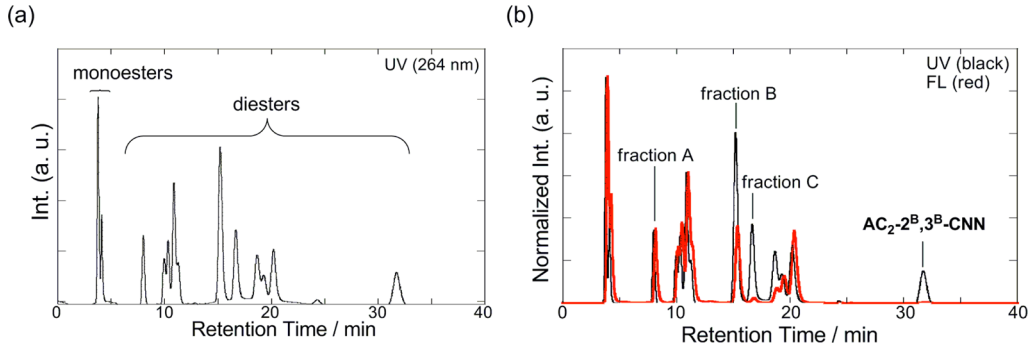

Figure 2. (a) Original and (b) normalized HPLC chromatograms of the crude products obtained by the esterification of AC and CNN with DCC/DMAP, monitored by (a) a UV detector (264 nm) and (b) UV (264 nm; black curve) and fluorescence (λ_{ex} = 254 nm, λ_{em} = 420 nm; red curve) detectors; the intensities were normalized at the largest monoester peak at 4 min.

Chart 3. Structures of $2^B,2^D$-Di-2-anthroyl-CNN (2^B2^D), $6^A,2^D$-Di-2-anthroyl-CNN (6^A2^D), and $6^A,2^B$-Di-2-anthroyl-CNN (6^A2^B)

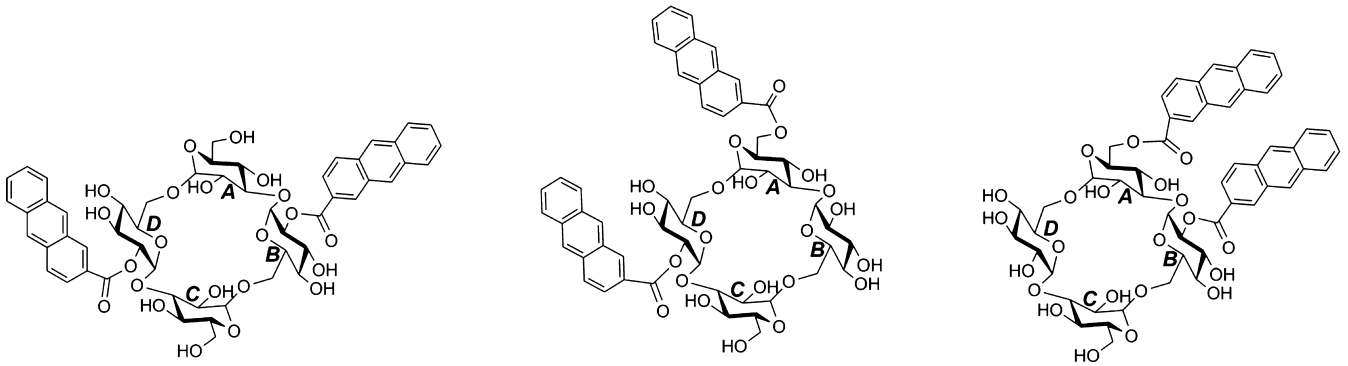

Table 1. Relative Yields of Regioisomeric AC_2-CNNs Isolated by HPLC

diester	2^B2^D	6^A2^D	6^A2^B	2^B3^B
relative yield[a]	14	42	24	20

[a]Determined by comparison of the peak areas of the chromatogram monitored by a UV detector at 264 nm, assuming equal extinction coefficients for all of the diesters.

each hydroxyl. For a more quantitative evaluation, the relative yields of the diesters were divided and distributed to each component hydroxyl to determine the relative contributions of the $2^B/2^D$-, 3^B-, and 6^A-hydroxyls as 29%/28%, 10%, and 33%, respectively; it should be noted that in this calculation the reactivities of these hydroxyls were assumed to be comparable before and after the first esterification, since these hydroxyls are not involved in the hydrogen-bonding network that defines the CNN conformation.[8b] Rather unexpectedly, the 6^A-hydroxyl is appreciably less reactive than the $2^B/2^D$-hydroxyl, which is not consistent with the monoesterification results, where the 6^A-monoester was favored by a factor of 1.81 over the 2^B-monoester (Figure 1), indicating that the second esterification of CNN has different selectivities and is more favorable for the primary hydroxyl.

Chiroptical Properties of AC- and AC_2-CNNs . The chiroptical properties of the four AC_2-CNNs and of monoester 6^A as a reference compound were examined in 45:55 CH_3CN/H_2O at room temperature. As shown in Figure 3a (top panel), the UV/vis spectra of 2^B2^D and 6^A2^D were essentially superimposable with each other (Figure S14 in the SI) and also with that of 6^A [except for the halved molar extinction coefficient (ε)], suggesting the absence of appreciable stacking interactions of ACs in diesters 2^B2^D and 6^A2^D in the ground state. Nevertheless, the CD spectra of 2^B2^D and 6^A2^D (Figure 3a, bottom) exhibited negative Cotton effects in the ^1B_b band that are much stronger than that observed for monoester 6^A, suggesting the existence of weak exciton-coupling interactions between the two AC chromophores on a CNN scaffold. Carrying two ACs on the adjacent or same nigerose ring(s), 6^A2^B and 2^B3^B behaved very differently from 2^B2^D and 6^A2^D (with two ACs located at more distant positions). As shown in Figure 3b (top panel), the UV/vis spectra of 6^A2^B and 2^B3^B suffered hypochromic effects with peak broadening compared with 2^B2^D and 6^A2^D (see Figure S14 in the SI for normalized UV/vis spectra and the related discussion). More crucially, the CD spectra of 6^A2^B and 2^B3^B exhibited intense exciton couplets in the ^1B_b band, the amplitudes of which amounted to 97 and 409 M^{-1} cm^{-1}, respectively. According to the exciton chirality theory,[11] the positive couplets observed indicate that the two AC chromophores on a CNN scaffold are aligned in a right-handed helical conformation on the average. In particular, the huge couplet observed for 2^B3^B is readily attributable to the ACs tethered to the vicinal 2,3-diol of ring B.[9]

NMR Spectra of AC- and AC_2-CNNs. Figure 4 compares the aromatic region of the NMR spectra of monoester 6^A and the four regioisomeric diesters 2^B2^D, 6^A2^D, 6^A2^B, and 2^B3^B. The chemical shift and coupling pattern of each aromatic proton in 2^B2^D and 6^A2^D are very close to each other and also to those of monoester 6^A. In contrast, all of the aromatic protons in 6^A2^B and 2^B3^B are more or less upfield-shifted (by 0.1−0.5 ppm) compared with those in 2^B2^D, 6^A2^D, and reference 6^A. More

dx.doi.org/10.1021/jo401977f | J. Org. Chem. 2013, 78, 10996−11006

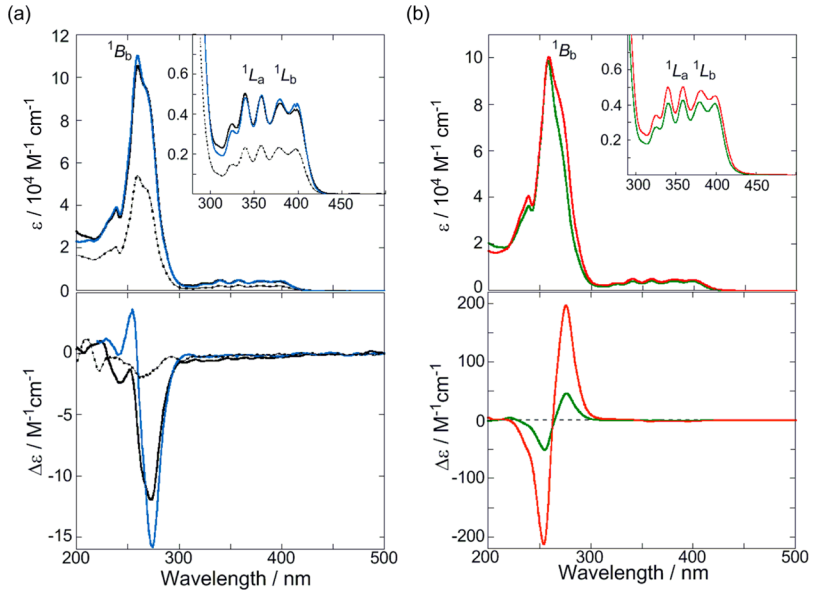

Figure 3. (top) UV/vis and (bottom) CD spectra of (a) 25 μM $\mathbf{6^A}$ (dotted black), 95 μM $\mathbf{2^B2^D}$ (black), and 39 μM $\mathbf{6^A2^D}$ (blue) and (b) 25 μM $\mathbf{6^A2^B}$ (green) and 45 μM $\mathbf{2^B3^B}$ (red) in 45:55 (v/v) CH_3CN/H_2O at room temperature, measured in a regular cell of 10 mm optical path.

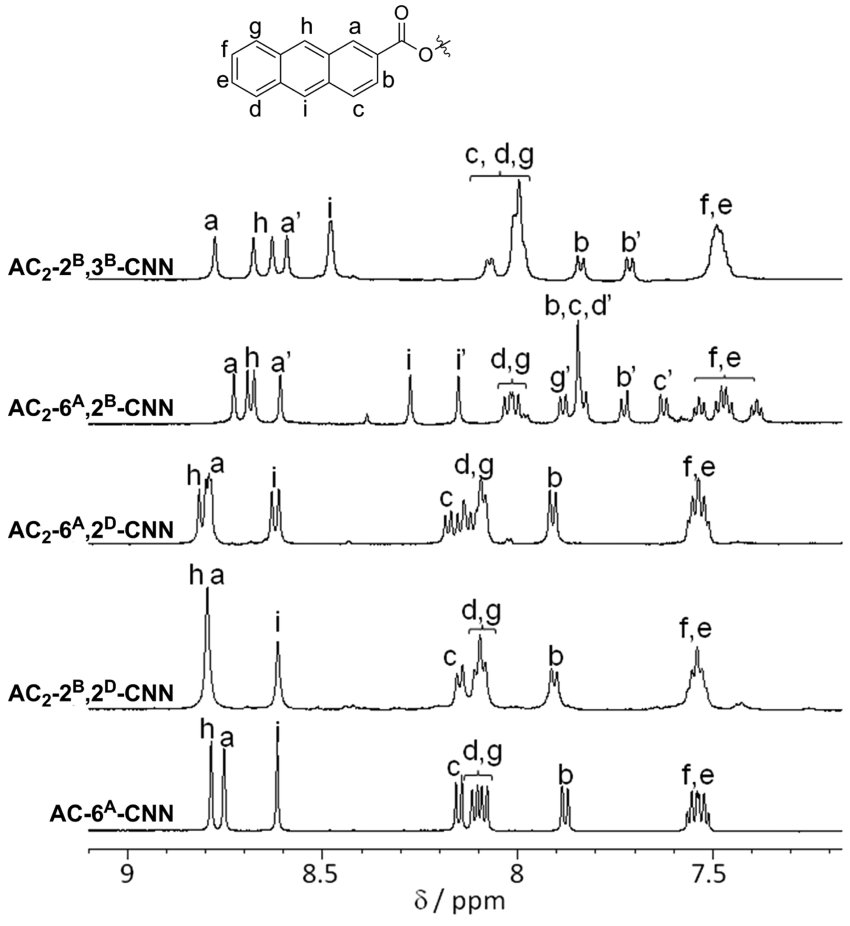

Figure 4. ^{1}H NMR spectra (aromatic region) of monoester $\mathbf{6^A}$ and the four regioisomeric diesters $\mathbf{2^B2^D}$, $\mathbf{6^A2^D}$, $\mathbf{6^A2^B}$, and $\mathbf{2^B3^B}$ in DMSO-d_6 at room temperature.

crucially, two formally equivalent aromatic protons at some specific positions are significantly split in $\mathbf{6^A2^B}$ and $\mathbf{2^B3^B}$ as a result of the stacking interaction that reduces the conformational freedom to magnetically differentiate the two ACs attached to different positions/rings of CNN. Thus, protons a and b of $\mathbf{2^B3^B}$ and protons c, d, and i of $\mathbf{6^A2^B}$ are remarkably split and upfield-shifted compared with the corresponding protons of $\mathbf{2^B2^D}$ and $\mathbf{6^A2^D}$, indicating partial overlap of the ACs

dx.doi.org/10.1021/jo401977f | J. Org. Chem. 2013, 78, 10996−11006

near the carbonyl in the former but closer overlap at the bottom half of the AC in the latter. These interpretations are compatible with the conclusion derived from the CD spectral examinations because the twist angle between the transition moments of the two ACs should be larger for the partially overlapped ACs in $2^{B}2^{D}$ than for the stacked ACs in $6^{A}2^{D}$. However, no appreciable cross-peaks were found for the split protons in the ROESY spectrum of $6^{A}2^{B}$, presumably because of the conformational flexibility of the side arm.

Fluorescence Spectra and Fluorescence Lifetimes of AC_2-CNNs. Fluorescence spectra of the four regioisomeric AC_2-CNNs (25 μM) were measured in a 45:55 mixture of CH_3CN and H_2O with excitation at 300 nm (where nearly equal absorbances were attained for all of the sample solutions used), and the observed fluorescence intensities were directly compared. As shown in Figure 5, the fluorescence spectra were

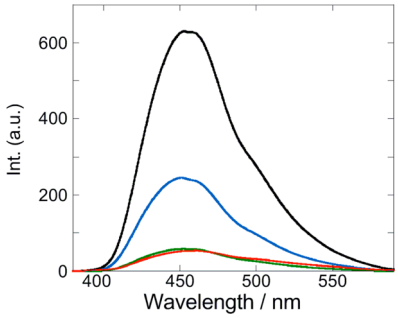

Figure 5. Fluorescence spectra of 25 μM solutions of $2^{B}2^{D}$ (black), $6^{A}2^{D}$ (blue), $6^{A}2^{B}$ (green), and $2^{B}3^{B}$ (red) in 45:55 CH_3CN/H_2O at room temperature; the excitation wavelength was tuned to 300 nm to achieve equal absorbance for all of the samples.

apparently similar to each other in shape, but the fluorescence intensity turned out to be a critical function of the position and ring on which each AC is introduced. Thus, the fluorescence intensities relative to $2^{B}2^{D}$ were found to be 0.4 for $6^{A}2^{D}$, 0.1 for $6^{A}2^{B}$, and 0.08 for $2^{B}3^{B}$. The order of decreasing fluorescence intensity qualitatively agrees with the order of increasing photocyclodimerization efficiency evaluated by the fluorescence versus UV spectral monitoring in HPLC analysis (Figure 2). This result indicates that the intramolecular photocyclodimerization of two ACs on the scaffold is fast enough to compete with the fluorescence and also that the inter-AC distance (and conformational freedom) on the scaffold determine the photocyclodimerization rate.

To confirm the competition between fluorescence and photocyclodimerization, the regioisomeric diesters were irradiated at 360 nm for 30−90 min (adjusted for the reactivity) in 45:55 CH_3CN/H_2O at 25 °C. As shown in Table 2, the conversion determined from the absorbance changes for the ^1L_a and ^1L_b bands (320−420 nm) was small (11%) for the most fluorescent $2^{B}2^{D}$ even after 90 min of irradiation but became much larger (45%) after 60 min of irradiation for the less fluorescent $6^{A}2^{D}$ and even larger for the least fluorescent $6^{A}2^{B}$ (75%) and $2^{B}3^{B}$ (57%) after 30 min of irradiation. Sensibly, $2^{B}2^{D}$ carrying the two ACs at the most distant positions on the transannular B and D rings was least reactive (and hence most fluorescent), while the other three diesters, with two ACs on the adjacent A/B or A/D rings or on the same B ring, reacted much faster. It should be noted, however, that $6^{A}2^{D}$ spectroscopically behaves very similarly to $2^{B}2^{D}$, showing no clear sign of stacking in CD (Figure 3a) or NMR (Figure 4),

Table 2. Photocyclodimerization and Fluorescence Efficiencies of Regioisomeric AC_2-CNNs

compound (μM)	irradiation time (min)	conversion (%)[a]	relative fluorescence intensity[b]
$2^{B}2^{D}$ (27)	90	11	≡1
$6^{A}2^{D}$ (27)	60	45	0.4
$6^{A}2^{B}$ (27)	30	75	0.1
$2^{B}3^{B}$ (29)	30	57	0.08

[a]Irradiated under N_2 at 360 ± 10 nm in 45:55 CH_3CN/H_2O at 25 °C with a 300 W xenon lamp through a bandpass filter. [b]See Figure 6 and the text.

but is much more reactive (and less fluorescent) than $2^{B}2^{D}$, indicating that the two ACs in $6^{A}2^{D}$ are not located close enough to stack in the ground state but have the conformational freedom to meet and cyclodimerize within the excited-state lifetime.

It is also intriguing that the order of decreasing fluorescence intensity does not entirely agree with the order of increasing reactivity, as $2^{B}3^{B}$ is slightly less fluorescent but obviously less reactive than $6^{A}2^{B}$ (Table 2), suggesting that additional photophysical decay path(s) are available to the former. To elucidate the origin of this apparent discrepancy, we first compared the shapes of the fluorescence spectra. As can be seen from Figure 6, the normalized fluorescence spectra of

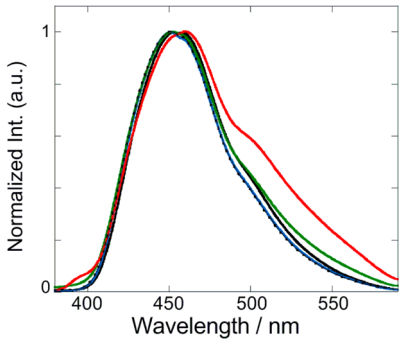

Figure 6. Normalized fluorescence spectra of 25 μM $2^{B}2^{D}$ (black), $6^{A}2^{D}$ (blue), $6^{A}2^{B}$ (green), $2^{B}3^{B}$ (red), and 6^{A} (dotted black) excited at 300 nm in 45:55 CH_3CN/H_2O at room temperature. All of the spectra have been normalized at the peak top.

$2^{B}2^{D}$, $6^{A}2^{D}$, and $6^{A}2^{B}$ are practically superimposable with that of monoester 6^{A}, while those of $2^{B}3^{B}$ and to a lesser extent $6^{A}2^{B}$ exhibit an appreciable deviation (tailing) at wavelengths above 480 and 510 nm, respectively, that is assignable to a new emission, presumably from an excimer, as the fluorescence excitation spectra measured at different monitoring wavelengths were essentially superimposable with each other and also with the relevant UV/vis spectra (Figure S15 in the SI). It is probably the case that the association of the two ACs is feasible but the subsequent cyclodimerization is conformationally less favorable and hence slower in $2^{B}3^{B}$ than in $6^{A}2^{B}$, allowing the intervention of such a short-lived excimer intermediate that radiatively and/or nonradiatively reverts to the ground state at the expense of the cyclodimerization yield.

To further elucidate the excited-state species generated upon irradiation and the subsequent photophysical and photochemical processes, we measured the fluorescence lifetimes of the mono- and diesters using the single-photon-counting technique. The fluorescence decay profiles of 6^{A} and $2^{B}2^{D}$

dx.doi.org/10.1021/jo401977f | J. Org. Chem. 2013, 78, 10996−11006

Table 3. Fluorescence Lifetimes of AC- and AC_2-CNNs[a]

compound (μM)	λ_{em} (nm)	n^b	τ_1	A_1	τ_2	A_2	τ_3	A_3	χ^2
$\mathbf{6}^{\mathbf{A}}$ (28)	450	1	21.6						1.0
	500	1	21.7						1.0
$\mathbf{2}^{\mathbf{B}}\mathbf{2}^{\mathbf{D}}$ (28)	450	1	21.3						0.9
	500	1	21.4						0.8
$\mathbf{6}^{\mathbf{A}}\mathbf{2}^{\mathbf{D}}$ (31)	450	2	5.2	0.55	18.2	0.45			1.0
	500	2	5.3	0.54	18.4	0.46			1.1
$\mathbf{6}^{\mathbf{A}}\mathbf{2}^{\mathbf{B}}$ (20)	450	3	0.3	0.74	3.9	0.08	15.2	0.18	1.0
	515	3	0.1	0.68	3.2	0.20	15.1	0.12	1.1
$\mathbf{2}^{\mathbf{B}}\mathbf{3}^{\mathbf{B}}$ (31)[c]	450	3	0.4	0.85	4.9	0.11	19.5	0.04	1.0
	515	3	0.4	0.52	5.2	0.43	19.0	0.05	1.1

[a]The fluorescence lifetime (τ_i, in ns) and relative abundance (A_i) of each component were determined by the single-photon-counting method in aqueous solution containing 45% CH_3CN at room temperature. [b]Number of components. [c]From ref 9.

Table 4. Product Distributions and Enantiomeric Excesses of Cyclodimers 1−4 Obtained by Photocyclodimerization of AC- and AC_2-CNNs[a]

					product distribution/% (ee/%)[c]				
compd (μM)	solvent	T (°C)	irradiation time (min)	conv. (%)[b]	**1**	**2***	**3***	**4**	HT:HH[d]
$\mathbf{6}^{\mathbf{A}}$ (46)	H_2O	25	120	40	41	25 (18)	25 (22)	9	66:34
$\mathbf{6}^{\mathbf{A}}$ (250)	H_2O (γ-CDx)[e]	25	15	55	32	34 (47)	22 (29)	12	66:34
$\mathbf{2}^{\mathbf{B}}\mathbf{2}^{\mathbf{D}}$ (27)	CH_3CN/H_2O[f]	25	90	11	27	16 (3)	40 (2)	17	43:57
$\mathbf{6}^{\mathbf{A}}\mathbf{2}^{\mathbf{D}}$ (27)	CH_3CN/H_2O[f]	25	60	45	10	9 (13)	71 (−18)	10	19:81
		10	60	29	11	9 (15)	69 (−14)	11	20:80
		−5	60	6	16	13 (21)	57 (−10)	14	29:71
$\mathbf{6}^{\mathbf{A}}\mathbf{2}^{\mathbf{D}}$ (133)				16	19	16 (21)	60 (−13)	5	35:65
$\mathbf{6}^{\mathbf{A}}\mathbf{2}^{\mathbf{B}}$ (27)	CH_3CN/H_2O[f]	25	30	75	2.9	1.5 (5)	45.7 (−62)	49.9	4:96
		10	30	68	0.7	0.1 (nd[g])	42.3 (−70)	56.9	1:99
		−5	30	62	1.3	0.4 (nd[g])	42.0 (−75)	56.3	2:98
	MeOH[h]	25	30	66	8	4 (8)	43 (−51)	45	12:88
		−50	30	64	2.0	0.9 (nd[g])	46.8 (−85)	50.3	3:97
		−70	30	64	0.5	0.2 (nd[g])	49.4 (−87)	49.9	1:99
$\mathbf{2}^{\mathbf{B}}\mathbf{3}^{\mathbf{B}}$ (29)[i]	CH_3CN/H_2O[f]	25	30	57	0.9	0.5 (nd[g])	96.3 (−99)	2.3	1:99
		−5	5	31	2.8	1.0 (nd[g])	94.4 (−98)	1.8	4:96

[a]Irradiated at 360 ± 10 nm under a N_2 atmosphere with a 300 W xenon lamp through a bandpass filter. [b]Determined by monitoring the absorbance change upon irradiation. [c]Irradiated samples were saponified [0.3 M KOH(aq), 24 h] and then subjected to chiral HPLC (ODS + Chiralcel OJ-RH) for determination of the product distribution and ee; the positive or negative ee value indicates dominant formation of the first- or second-eluted *M* or *P* enantiomer, respectively (ref 12); errors are ±1% for the product distributions and ±2% for the ee values. [d]HT:HH = ([**1**] + [**2***]):([**3***] + [**4**]). [e]γ-Cyclodextrin (0.625 mM) was added. [f]A 45:55 mixture of acetonitrile and water. [g]Not determined. [h]Concentration was determined using the value of ε in a 45:55 mixture of acetonitrile and water. [i]From ref 9.

measured at 450 nm and 500 or 515 nm were nicely fitted to a single-exponential function to give practically identical lifetimes (τ) of 21−22 ns (Table 3; see Figure S16 in the SI for the decay profiles and the fitting results). This seems reasonable, since the two ACs tethered to the 2-positions of the remote B and D rings in $\mathbf{2}^{\mathbf{B}}\mathbf{2}^{\mathbf{D}}$ are equivalent to each other and geometrically no stacking interaction is expected to occur in the excited state.

However, the fluorescence decay of $\mathbf{6}^{\mathbf{A}}\mathbf{2}^{\mathbf{D}}$ obviously contained multiple components and was fitted to a sum of two exponential functions to give distinct lifetimes of 18 and 5 ns with reasonable χ^2 values. Despite the distinctly different lifetimes, the relative abundance (A_1/A_2) did not change when the monitoring wavelength was altered from 450 to 500 nm, indicating that the fluorescence spectra of these two species are very similar to each other in energy and shape. A simplest rationalization of these results would be to assume that two ACs introduced at the 2- and 6-positions of the adjacent D and A rings in $\mathbf{6}^{\mathbf{A}}\mathbf{2}^{\mathbf{D}}$ are inherently nonequivalent and give different lifetimes. However, this is readily ruled out by the fact that the lifetimes of the ACs introduced at the 6-position of $\mathbf{6}^{\mathbf{A}}$ and the 2-position of $\mathbf{2}^{\mathbf{B}}\mathbf{2}^{\mathbf{D}}$ are essentially the same and longer than those obtained for $\mathbf{6}^{\mathbf{A}}\mathbf{2}^{\mathbf{D}}$. It is also difficult to assign one lifetime to free AC and the other to an excimer, since no extra emission at longer wavelengths was observed and no rise was observed in the fluorescence decay profiles. The major difference of the ACs in $\mathbf{6}^{\mathbf{A}}\mathbf{2}^{\mathbf{D}}$ from those in $\mathbf{6}^{\mathbf{A}}$ and $\mathbf{2}^{\mathbf{B}}\mathbf{2}^{\mathbf{D}}$ is the intramolecular accessibility, which allows dynamic quenching of an excited AC by another AC on the CNN scaffold of $\mathbf{6}^{\mathbf{A}}\mathbf{2}^{\mathbf{D}}$. The rate of intramolecular dynamic quenching may differ for conformational isomers.[9] The excitations of the 6^A-AC and 2^D-AC are likely to occur with equal probability, but the rates of the subsequent quenching by ground-state 2^D-AC and 6^A-AC, respectively, may differ, affording distinct fluorescence lifetimes as observed experimentally. The dynamic quenching leads to photocyclodimerization, probably via exciplex intermediate(s), which are however extremely short-lived and/or nonfluorescent, as no additional emission or lifetime was observed.

In the case of $\mathbf{6}^{\mathbf{A}}\mathbf{2}^{\mathbf{B}}$ and $\mathbf{2}^{\mathbf{B}}\mathbf{3}^{\mathbf{B}}$, the fluorescence decay could not be analyzed using single- or double-exponential functions

dx.doi.org/10.1021/jo401977f | J. Org. Chem. 2013, 78, 10996−11006

but could be fitted only to a sum of three exponential functions to give three distinct lifetimes of <1, 3−5, and 15−19 ns with relative abundances that varied appreciably with monitoring wavelength, as shown in Table 3. In our recent study of the fluorescence behavior of $\mathbf{2}^{\mathbf{B}}\mathbf{3}^{\mathbf{B}}$,[9] we elucidated that these three species with distinct lifetimes (τ_1−τ_3) are assignable to "*in*−*in*", "*in*−*out*", and "*out*−*out*" conformers with respect to the rotation around the aroyl bond. The shortest lifetime (τ_1) and longest lifetime (τ_3) are attributed to the *in*−*in* and *out*−*out* conformers, respectively, which differ in geometry and exhibit very contrasting fluorescence behavior. Thus, the two ACs are located very close together in the former, causing extremely fast dynamic quenching, but separated in space in the latter, discouraging the quenching. On the other hand, the intermediate τ_2 is assigned to the *in*−*out* conformer, which forms a partially overlapped excimer (the origin of the extra fluorescence observed at longer wavelengths for $\mathbf{2}^{\mathbf{B}}\mathbf{3}^{\mathbf{B}}$; Figure 6, red line), and hence, its abundance A_2 remarkably increases upon monitoring at 515 nm. The fluorescence spectral and fluorescence lifetime behaviors of $\mathbf{6}^{\mathbf{A}}\mathbf{2}^{\mathbf{B}}$ (Figure 6, green line) are very similar to those of $\mathbf{2}^{\mathbf{B}}\mathbf{2}^{\mathbf{D}}$, and hence, the same mechanisms and species are deduced to be involved.

Diastereodifferentiating Photocyclodimerization. Photoirradiation of AC- and AC_2-CNNs was performed at 360 nm in aqueous solution at temperatures ranging from 25 to −5 °C and/or in methanol at temperatures ranging from 25 to −70 °C with UV/vis monitoring. The irradiated samples were saponified with aqueous KOH, and the resulting solutions containing liberated AC dimers **1**−**4** and unreacted AC were analyzed by chiral HPLC to give the product distributions and the ee's for **2*** and **3***, as shown in Table 4.

The CNN moiety in $\mathbf{6}^{\mathbf{A}}$ functions as a chiral auxiliary to control the stereochemical outcome of the photocyclodimerization of AC tethered to CNN, as was the case with the conventional diastereodifferentiating photoreactions controlled by chiral substituents.[10,13] Despite the apparently bulky CNN auxiliary tethered to AC, the head-to-tail/head-to-head (HT/HH) ratio obtained was modest (66:34), and the ee was rather low (18% for **2*** and 22% for **3***), indicating that the steric bulk of CNN tethered to AC through an ester linkage cannot effectively provide stereocontrol of the intermolecular photocyclodimerization of the tethered AC. For better stereocontrol, we decided to apply the dual supramolecular approach[7b,c] by adding γ-CDx to the present system using CNN as a chiral auxiliary. As shown in Figure 7, UV/vis spectral examinations revealed significant hypochromic and appreciable bathochromic effects in the ^1B_b, ^1L_a, and ^1L_b bands upon gradual addition of γ-CDx up to a concentration of 0.625 mM (at which the change was almost saturated, suggesting full complexation), while the CD spectra showed a dramatic change from a simple negative Cotton effect to a positive exciton couplet at the ^1B_b band; both indicate inclusion of two AC moieties in the γ-CDx cavity. A much shorter photoirradiation time was required for the aqueous solution containing $\mathbf{6}^{\mathbf{A}}$ (0.25 mM) and γ-CDx (0.625 mM) compared with that for $\mathbf{6}^{\mathbf{A}}$ alone (by a factor of ca. 10) as a result of the intracomplex photocyclodimerization. Although the HT/HH ratio was identical to that obtained without γ-CDx, the enantioselectivity was enhanced from 18% to 47% ee for **2*** and from 22% to 29% ee for **3*** through complexation with γ-CDx.

The photocyclodimerization of $\mathbf{2}^{\mathbf{B}}\mathbf{2}^{\mathbf{D}}$ in aqueous acetonitrile at 25 °C was slower than that of $\mathbf{6}^{\mathbf{A}}$ (after a correction for the difference in absorbance due to the lower concentration),

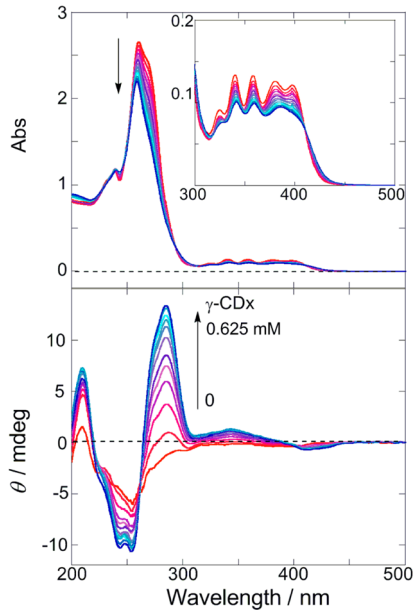

Figure 7. (top) UV/vis and (bottom) CD spectral changes of an aqueous solution of $\mathbf{6}^{\mathbf{A}}$ (0.25 mM) upon gradual addition of γ-CDx (0, 0.025, 0.050, 0.075, 0.1, 0.125, 0.175, 0.225, 0.275, 0.325, 0.425, 0.625 mM from red to blue) at room temperature, measured in a 2 mm cell.

probably because of the steric hindrance around the ACs introduced at the 2-position rather than the 6-position. The product selectivity was only slightly HH-favored (HT:HH = 43:57), and the enantioselectivity was very low (2−3% ee) for both **2*** and **3***, suggesting the intermolecular nature of the photocyclodimerization. This is totally comparable with the results of the CD spectral and fluorescence lifetime examinations that revealed practically no ground- or excited-state intramolecular interactions between the two AC moieties on the B and D rings of CNN. The photocyclodimerization of $\mathbf{2}^{\mathbf{B}}\mathbf{2}^{\mathbf{D}}$ possessing two ACs on the distant B and D rings of CNN is deduced to be almost exclusively intermolecular and therefore proceeds slowly and less stereoselectively. AC tethered at the 6-position of nigerose appears to give a better ee with a higher HT/HH selectivity than that at the 2-position.

The photocyclodimerization of $\mathbf{6}^{\mathbf{A}}\mathbf{2}^{\mathbf{D}}$ proceeded much faster than those of $\mathbf{6}^{\mathbf{A}}$ and $\mathbf{2}^{\mathbf{B}}\mathbf{2}^{\mathbf{D}}$ to afford **3*** in 71% yield with a high HH selectivity of 81%, although the ee's were modest (10−21%) for both **2*** and **3***. The efficient photocyclodimerization indicates that two ACs at the 6- and 2-positions of the adjacent A and D rings of CNN become accessible intramolecularly on the scaffold in an *anti*-HH fashion, probably as a result of the adjacent A and D rings with a longer and more flexible hydroxymethyl linker at the 6^A-position. When the temperature was reduced to −5 °C, the HH selectivity was slightly decreased to 71%, suggesting that the thermodynamically favored *anti*-HH conformer is photochemically less reactive (kinetically disfavored), probably as a result of the energetically demanding conformational changes required upon cyclodimerization. The yet lower HH selectivity of 65% obtained upon photodimerization of $\mathbf{6}^{\mathbf{A}}\mathbf{2}^{\mathbf{D}}$ at a 5-fold higher concentration (0.133 mM) suggests the existence of the intermolecular route to HT dimers. The ee's of **2*** and **3*** were modest but exhibited apparently opposite temperature-dependence behaviors: reducing the temperature led to higher ee's for the former but lower ee's for the latter. The Eyring plot of the relative formation rate of the *M* versus *P* enantiomer,[12] $k_M/k_P = k_+/k_- =$

dx.doi.org/10.1021/jo401977f | J. Org. Chem. 2013, 78, 10996−11006

[100 + (% ee)]/[100 − (% ee)], gave a straight line for both **2*** and **3*** (Figure 8), meaning that a single diastereodifferentiation mechanism operates over the entire temperature range employed. From the slope and intercept of the plot, the differential activation parameters were calculated as $\Delta\Delta H^{\ddagger}$ = −3.7 kJ mol^{-1} and $\Delta\Delta S^{\ddagger}$ = −10.3 J mol^{-1} K^{-1} for **2*** and $\Delta\Delta H^{\ddagger}$ = −3.6 kJ mol^{-1} and $\Delta\Delta S^{\ddagger}$ = −15.1 J mol^{-1} K^{-1} for **3***. Both $\Delta\Delta H^{\ddagger}$ and $\Delta\Delta S^{\ddagger}$ are negative, and the values indicate that the formation of the *M* enantiomer is favored enthalpically to a similar degree for **2*** and **3*** but disfavored entropically to a larger degree for the latter. It is noteworthy that the difference in $\Delta\Delta S^{\ddagger}$ is decisive and solely responsible for the opposite sign of the ee value for **2*** versus **3***, while the $\Delta\Delta H^{\ddagger}$ values are essentially the same. Furthermore, the different $\Delta\Delta S^{\ddagger}$ and identical $\Delta\Delta H^{\ddagger}$ values indicate that the diastereodifferentiation steps for **2*** and **3*** differ in conformational freedom but are similar in steric energy, suggesting intervention of distinct conformers that do not equilibrate within the lifetime.

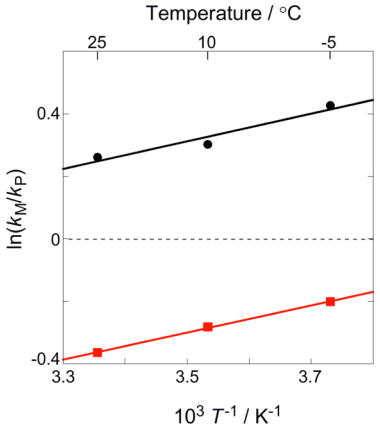

Figure 8. Eyring plots of the relative rate constant k_M/k_P for the formation of (*M*)- and (*P*)-**2*** (circles) and **3*** (squares) in the diastereodifferentiating photocyclodimerization of $\mathbf{6^A2^D}$.

Crucially, the photocyclodimerization of $\mathbf{6^A2^B}$ was the fastest among the AC- and AC_2-CNNs examined and afforded almost exclusively the *anti*- and *syn*-HH dimers in 96−99% combined yield, indicating highly efficient intramolecular photocyclodimerization of the two ACs tethered to the 6^A- and 2^B-positions of CNN, which are closer by three C−C/C−O bonds than those on the 6^A- and 2^D-positions (see Chart 3). Although the *anti*/*syn* selectivity was low at near unity, the ee of the *anti*-HH dimer **3*** was much better than those obtained for $\mathbf{6^A}$, $\mathbf{2^B2^D}$, and $\mathbf{6^A2^D}$ and enhanced up to −75% when the temperature was reduced to −5 °C. Hence, we performed the photocyclodimerization in methanol to obtain **3*** with −87% ee in 49% yield at −70 °C. By application of the Eyring equation to the temperature-dependent ee values of **3*** in aqueous acetonitrile and in methanol (Table 4 and Figure 9), the differential activation parameters for the diastereodifferentiating photocyclodimerization of $\mathbf{6^A2^B}$ were calculated as $\Delta\Delta H^{\ddagger}$ = 10.9 kJ mol^{-1} and $\Delta\Delta S^{\ddagger}$ = 24.5 J mol^{-1} K^{-1} for aqueous acetonitrile and $\Delta\Delta H^{\ddagger}$ = 9 kJ mol^{-1} and $\Delta\Delta S^{\ddagger}$ = 19 J mol^{-1} K^{-1} for methanol (less accurate because of the scatter in the plot). The differential enthalpy and entropy values compensate for each other (a plot of $\Delta\Delta H^{\ddagger}$ against $\Delta\Delta S^{\ddagger}$ passes through the origin), suggesting that a common diastereodifferentiation mechanism is operative in the two solvents. The small differences in both $\Delta\Delta H^{\ddagger}$ and $\Delta\Delta S^{\ddagger}$ are jointly responsible for the appreciably different ee values and temperature-dependence behaviors in the two solvents. Examination of the CD spectra of $\mathbf{6^A2^B}$ in the two solvents (Figure S17 in the SI) revealed that the anisotropy factor ($g = \Delta\varepsilon/\varepsilon$) is much larger in aqueous acetonitrile than in methanol, suggesting less flexible conformations in the former solvent, presumably because of the heavy solvation by water molecules.

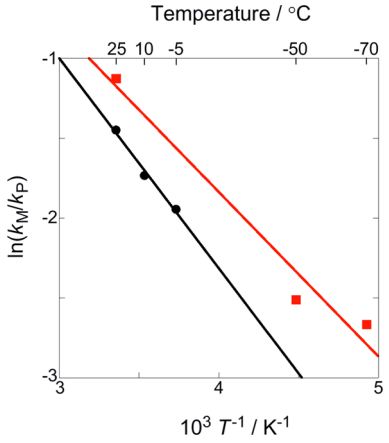

Figure 9. Eyring plots of the relative rate constant k_M/k_P for the formation of (*M*)- and (*P*)-**3*** in the diastereodifferentiating photocyclodimerization of $\mathbf{6^A2^B}$ in 45:55 CH_3CN/H_2O (circles) and in methanol (squares).

As reported in our recent communication,[9] photocyclodimerization of $\mathbf{2^B3^B}$ proceeded very efficiently with nearly perfect stereocontrol to give practically enantiopure **3*** (−99% ee) in 96% yield. This is noteworthy, as simultaneously achieving chemical and optical yields at such a high level is rare in conventional photochirogenesis.[2−6] The achievement of the unprecedentedly efficient *anti*/*syn*, HH/HT, and diastereocontrol is attributable to the equatorial 2,3-diol scaffold on the rigid CNN skeleton, which thermodynamically drives the two AC moieties of $\mathbf{2^B3^B}$ to the *in*−*in* conformer in the ground state and kinetically facilitates the cyclodimerization in the excited state. Obviously, the thermodynamics alone is not sufficient to shift the conformer distribution in the ground state to a single conformer. Indeed, the fluorescence lifetime study revealed the existence of at least three fluorescent species in the solution (Table 3). It is therefore likely that the nearly perfect stereocontrol was achieved not only by narrowing the ground-state conformer distribution but also by manipulating the photocyclodimerization efficiencies of the dynamically equilibrating conformers by tethering two ACs to the vicinal positions of the rigid CNN with a short linker.

■ CONCLUSION

In this study, four regioisomeric AC_2-CNNs of varying intramolecular photocyclodimerization ability were selectively isolated from a complex esterification mixture of CNN by carefully choosing photoinert ($\mathbf{2^B2^D}$), moderately photoreactive ($\mathbf{6^A2^D}$), and highly photoreactive ($\mathbf{6^A2^B}$ and $\mathbf{2^B3^B}$) peaks detected on an HPLC system equipped with tandem UV and fluorescence monitors. UV/vis, CD, and NMR spectral examinations of these AC_2-CNNs revealed the close proximity of the two AC chromophores, particularly in $\mathbf{6^A2^B}$ and $\mathbf{2^B3^B}$. Fluorescence spectral and lifetime studies showed the existence of dynamically equilibrating conformers that substantially differ in photocyclodimerization efficiency and play a decisive role in

dx.doi.org/10.1021/jo401977f | J. Org. Chem. 2013, 78, 10996−11006

determining the stereochemical outcomes of photocyclodimerization along with the ground-state population of each conformer. As a consequence of the spatial proximity and favorable conformation of two ACs on the CNN scaffold, 6^A2^B and 2^B3^B photocyclodimerized most rapidly to afford exclusively the HH dimers in 99% combined yields with poor *anti*/*syn* selectivity (1:1) for the former substrate but excellent **3*** selectivity for the latter. The vicinal diol scaffold on the rigid CNN skeleton may be widely used as a promising tool for obtaining high chemical and optical yields in various photochemical, and probably thermal, dimerization and addition reactions. The new insights into the factors and mechanisms that control the chirogenic processes in both the ground and excited states will provide a clearer view and reliable tools for designing and understanding a new photochirogenic system. Further studies to find less sophisticated chiral scaffolds that can afford equally high chemical and optical yields are currently in progress.

EXPERIMENTAL SECTION

Instruments. ^{1}H NMR spectra at 600 MHz, ^{13}C NMR spectra at 150 MHz, and 2D HSQC and COSY spectra at 600 MHz were recorded in DMSO-d_6. UV/vis and CD spectra were measured in a quartz cell (with a light path of 2 or 10 mm) equipped with a temperature controller. Fluorescence lifetimes were determined by the time-correlated single-photon-counting method using a pulsed H_2 light source. HPLC analyses of the product distribution and ee of cyclodimers were performed at 35 °C on a tandem column eluted with a 64:36 (v/v) mixture of deionized water and acetonitrile containing 0.1% trifluoroacetic acid at a flow rate of 0.5 mL min^{-1}.

Materials. Commercially available fluorescence-free acetonitrile and water were used without further purification. Cyclic nigerosylnigerose (CNN) was supplied by Hayashibara Co., Ltd.

Spectroscopy. A given amount of AC- or AC_2-CNN was dissolved in 45:55 CH_3CN/H_2O or MeOH, and the resulting solution was placed in a quartz cell (2 or 10 mm path length) and subjected to UV/vis, CD, and fluorescence spectral examinations and fluorescence lifetime measurements at room temperature.

Photolyses and Saponification. An aqueous acetonitrile or methanol solution of AC-modified CNN was irradiated under a nitrogen atmosphere at various temperatures in a quartz cell (10 mm × 10 mm × 45 mm) using a 300 W xenon lamp fitted with a bandpass filter (360 ± 10 nm). The irradiated solution thus obtained was hydrolyzed for 24 h by addition of KOH (0.3 M), and the resulting solution was subjected to chiral HPLC analysis.

Preparation of AC- and AC_2-CNNs. CNN (1.0 g, 1.5 mmol) was dissolved in dry DMF (50 mL), and to the solution were added *N*,*N*′-dicyclohexylcarbodiimide (DCC) (701 mg, 3.4 mmol) and 4-(*N*,*N*-dimethylamino)pyridine (DMAP) (415 mg, 3.4 mmol) under nitrogen. After the complete dissolution of the reagents, 2-anthracenecarboxylic acid (999 mg, 4.5 mmol) was added, and the mixture was stirred for 24 h under nitrogen at room temperature. After removal of urea (byproduct) by filtration, the filtrate was slowly poured onto diethyl ether (450 mL) and stirred for 2 h to give a precipitate, which was collected by filtration, washed with diethyl ether, and dried in vacuo to give the crude product as a yellow solid (720 mg). The crude product was a mixture of CNN and mono-, di-, and tri-AC-esters in a ca. 1:2:1:0.1 ratio as estimated from the MALDI-TOF-MS spectrum without taking into account the difference in ionization efficiency (see Figure S1c in the SI).

Characterization of AC- and AC_2-CNNs. *Monoester* 2^B. Mp >250 °C (decomposition). ^{1}H NMR (DMSO-d_6, 600 MHz, 25 °C): δ_H 8.79 (2H, s), 8.61 (1H, s), 8.14 (1H, d, J = 9.0 Hz), 8.10−8.08 (2H, m), 7.90 (1H, d, J = 10.0 Hz), 7.56−7.51 (2H, m), 5.62 (1H, d, J = 4.0 Hz, B_1), 5.30 (1H, d, J = 4.1 Hz, D_1), 4.75 (1H, dd, J = 10.1, 4.1 Hz, B_2), 4.64 (1H, t, J = 10.4 Hz), 4.59 (1H, d, J = 3.4 Hz), 4.57 (1H, d, J = 3.6 Hz), 4.49−4.46 (1H, m, overlapped with OH peaks), 3.86−3.77 (3H, m), 3.59−3.12 (16H, m), 3.06−3.02 (1H, m), 2.82−2.78 (1H, m). ^{13}C NMR (DMSO-d_6, 150 MHz, 25 °C): δ_C 166.1 (C═O), 133.0, 132.6, 132.4, 132.0, 130.3, 129.1, 129.0, 128.8, 128.6, 127.5, 127.3, 126.6, 124.5, 100.5, 100.3, 97.3, 95.3, 76.2, 76.1, 74.6, 73.3, 73.0, 72.8, 72.7, 71.9, 71.6, 71.6, 71.5, 71.0, 70.9, 70.8, 70.5, 70.1, 69.3, 69.2, 61.0, 60.6. HR-MS (MALDI-TOF) m/z: [M + Na]$^+$ calcd for $C_{39}H_{48}O_{21}Na$ 875.2586, found 875.2620.

Monoester 6^A. Mp >260 °C (decomposition). ^{1}H NMR (DMSO-d_6, 600 MHz, 25 °C): δ_H 8.79 (1H, s), 8.75 (1H, s), 8.62 (1H, s), 8.15 (1H, d, J = 9.0 Hz), 8.12−8.08 (2H, m), 7.88 (1H, dd, J = 8.8, 1.2 Hz), 7.56−7.51 (2H, m), 5.35 (1H, d, J = 3.9 Hz), 5.33 (1H, d, J = 4.0 Hz), 4.66 (1H, d, J = 3.5 Hz), 4.56 (1H, d, J = 3.5 Hz), 4.53−4.32 (4H, m), 4.13 (1H, d, J = 9.0 Hz), 3.87 (1H, t, J = 9.3 Hz), 3.82−3.77 (2H, m), 3.59−3.15 (14H, m), 2.87−2.80 (2H, m, B_4, D_4). ^{13}C NMR (DMSO-d_6, 150 MHz, 25 °C): δ_C 166.1 (C═O), 133.1, 132.5, 132.2, 132.1, 130.2, 129.3, 129.2, 128.9, 128.5, 127.4, 127.0, 126.7, 124.0, 100.3, 97.9, 76.1 (C_3), 75.8 (A_3), 73.9 (C_5), 72.9, 72.7 (C_2), 71.7, 71.6, 71.0, 70.8 (A_2), 70.2, 70.0, 69.9, 69.4, 69.3, 64.4 (A_6), 61.0 (C_6). HR-MS (FAB) m/z: [M + Na]$^+$ calcd for $C_{39}H_{48}O_{21}Na$ 875.2586, found 875.2613.

Diester 2^B2^D. Mp >269 °C (decomposition). ^{1}H NMR (DMSO-d_6, 600 MHz, 25 °C): δ_H 8.80 (4H, s), 8.62 (2H, s), 8.15 (2H, d, J = 8.6 Hz), 8.11−8.08 (4H, m), 7.91 (2H, d, J = 8.9 Hz), 7.56−7.52 (4H, m), 5.62 (2H, d, J = 3.6 Hz, B_1, D_1), 4.75 (2H, dd, J = 10.0, 3.7 Hz, B_2, D_2), 4.65 (2H, m, B_5, D_5), 4.62 (2H, d, J = 2.9 Hz, A_1, C_1), 3.86−3.83 (4H, m, A_3, B_3, C_3, D_3), 3.58−3.10 (14H, m), 3.04 (2H, t, J = 9.2 Hz, B_4, D_4). ^{13}C NMR (DMSO-d_6, 150 MHz, 25 °C): δ_C 166.1 (C═O), 133.1, 132.6, 132.4, 132.0, 130.3, 129.1, 129.0, 128.8, 128.6, 127.5, 127.3, 126.6, 124.5, 100.4 (A_1, C_1), 95.3 (B_1, D_1), 76.3 (B_3, D_3), 74.6 (B_2, D_2), 72.9, 71.9, 71.6 (B_4, D_4), 71.1 (A_3, C_3), 70.8, 70.5 (B_5, D_5), 69.2 (B_6, D_6), 60.6 (A_6, C_6). HR-MS (MALDI-TOF) m/z: [M + Na]$^+$ calcd for $C_{54}H_{56}O_{22}Na$ 1079.3161, found 1079.3129.

Diester 6^A2^D. Mp >243 °C (decomposition). ^{1}H NMR (DMSO-d_6, 600 MHz, 25 °C): δ_H 8.82−8.79 (4H, m), 8.63 (1H, s), 8.61 (1H, s), 8.19−8.08 (6H, m), 7.91 (2H, d, J = 8.8 Hz), 7.55−7.51 (4H, m), 5.66 (1H, d, J = 3.8 Hz, D_1), 5.36 (1H, d, J = 3.7 Hz, B_1), 4.80 (1H, dd, J = 10.1, 3.7 Hz, D_2), 4.71−4.69 (2H, m), 4.59 (1H, d, J = 3.1 Hz, C_1), 4.52−4.30 (3H, m), 3.90−3.82 (4H, m), 3.68 (1H, t, J = 9.8 Hz), 3.61−3.57 (2H, m), 3.48−3.18 (10H, m), 3.06 (1H, t, J = 9.4 Hz), 2.82 (1H, t, J = 9.2 Hz). ^{13}C NMR (DMSO-d_6, 150 MHz, 25 °C): δ_C 166.2 (C═O), 133.1, 133.1, 132.6, 132.4, 132.2, 132.1, 132.0, 130.3, 129.3, 129.2, 129.1, 129.0, 128.9, 128.8, 128.6, 127.5, 127.4, 127.3, 127.0, 127.7, 126.6, 124.5, 124.1, 100.3 (A_1), 100.3 (C_1), 98.0 (B_1), 95.3 (D_1), 76.3 (D_3), 75.9 (A_3), 74.6 (D_2), 73.9, 72.8 (C_2), 72.7 (B_2), 71.9, 71.8 (D_4), 71.5 (A_4), 71.0, 70.8 (A_2), 70.3 (D_5), 70.2, 70.0 (A_5), 69.3 (B_6), 69.2 (D_6), 64.4 (A_6), 60.6 (C_6). HR-MS (MALDI-TOF) m/z: [M + Na]$^+$ calcd for $C_{54}H_{56}O_{22}Na$ 1079.3161, found 1079.3215.

Diester 6^A2^B. Mp >243 °C (decomposition). ^{1}H NMR (DMSO-d_6, 600 MHz, 25 °C): δ_H 8.73 (1H, s), 8.69 (1H, s), 8.68 (1H, s), 8.61 (1H, s), 8.28 (1H, s), 8.15 (1H, s), 8.03−7.97 (2H, m), 7.88 (1H, d, J = 8.3 Hz), 7.85−7.82 (3H, m), 7.73 (1H, d, J = 9.2 Hz), 7.63 (1H, d, J = 10.0 Hz), 7.54 (1H, t, J = 7.2 Hz), 7.47 (2H, q, J = 7.9 Hz), 7.39 (1H, t, J = 7.6 Hz), 5.64 (1H, d, J = 3.8 Hz, B_1), 5.30 (1H, d, J = 3.8 Hz, D_1), 4.75 (1H, dd, J = 4.0, 10.1 Hz, B_2), 4.65 (1H, d, J = 3.4 Hz, A_1), 4.63−4.59 (1H, m, B_5), 4.57 (1H, d, J = 3.5 Hz, C_1), 4.48 (1H, t, J = 9.9 Hz), 4.33 (1H, d, J = 10.5 Hz), 4.24−4.22 (1H, m), 3.89 (1H, t, J = 9.2 Hz, A_3), 3.83 (1H, t, J = 9.3 Hz, B_3), 3.78 (1H, t, J = 8.9 Hz, C_3), 3.57−3.13 (14H, m), 3.03 (1H, t, J = 9.3 Hz, B_4), 2.81 (1H, t, J = 9.7 Hz, D_4). ^{13}C NMR (DMSO-d_6, 150 MHz, 25 °C): δ_C 166.1 (C═O), 166.0 (C═O), 133.1, 132.9, 132.4, 132.4, 132.1, 132.0, 131.9, 130.2, 130.1, 129.1, 129.0, 128.9, 128.8, 128.5, 128.4, 127.6, 127.4, 127.2, 126.9, 126.7, 126.5, 126.3, 124.5, 123.8, 100.4 (C_1), 100.3 (A_1), 97.9 (D_1), 95.3 (B_1), 76.2 (C_3), 75.9 (A_3), 74.5 (B_2), 73.9, 72.9 (C_4), 72.7 (D_2), 71.9 (A_4), 71.6 (B_4), 71.5, 71.1 (B_3), 70.9 (C_2), 70.6 (A_2), 70.5 (B_5), 70.0, 69.9 (A_5), 69.4 (D_6), 69.1 (B_6), 64.2 (A_6), 61.0 (C_6). HR-MS (MALDI-TOF) m/z: [M + Na]$^+$ calcd for $C_{54}H_{56}O_{22}Na$ 1079.3161, found 1079.3185.

dx.doi.org/10.1021/jo401977f | J. Org. Chem. 2013, 78, 10996−11006

■ ASSOCIATED CONTENT

Supporting Information

HPLC analyses; MS, NMR, UV, CD, and fluorescence excitation spectra; and fluorescence lifetimes of modified CNNs. This material is available free of charge via the Internet at http://pubs.acs.org.

■ AUTHOR INFORMATION

Corresponding Authors

*E-mail: gaku@chem.eng.osaka-u.ac.jp (G.F.).
*E-mail: inoue@chem.eng.osaka-u.ac.jp (Y.I.).

Notes

The authors declare no competing financial interest.

■ ACKNOWLEDGMENTS

G.F. appreciates the generous support by a Grant-in-Aid for Young Scientists (B) (23750129) from the Japan Society for the Promotion of Science (JSPS) and also by the Iwatani Naoji Foundation and the Sumitomo Foundation. Y.I. is thankful for the support of this work by a Grant-in-Aid for Scientific Research (A) (21245011) from JSPS. Y.C. thanks the National Natural Science Foundation of China (NSFC) (Grant 21372165).

■ REFERENCES

(1) (a) Inoue, Y. *Chem. Rev.* **1992**, *92*, 741. (b) Griesbeck, A. G.; Meierhenrich, U. J. *Angew. Chem., Int. Ed.* **2002**, *41*, 3147. (c) *Chiral Photochemistry*; Inoue, Y., Ramamurthy, V., Eds.; Marcel Dekker: New York, 2004. (d) Müller, C.; Bach, T. *Aust. J. Chem.* **2008**, *61*, 557. (e) Hoffmann, N. *Chem. Rev.* **2008**, *108*, 1052. (f) *Supramolecular Photochemistry*; Ramamurthy, V., Inoue, Y., Eds.; Wiley: New York, 2011.

(2) (a) Martin, R. H. *Chimia* **1975**, *29*, 137. (b) Yokoyama, Y.; Shiozawa, T.; Tani, Y.; Ubukata, T. *Angew. Chem., Int. Ed.* **2009**, *48*, 4521.

(3) (a) Inoue, T.; Matsuyama, K.; Inoue, Y. *J. Am. Chem. Soc.* **1999**, *121*, 9877. (b) Matsuyama, K.; Inoue, T.; Inoue, Y. *Synthesis* **2001**, 1167.

(4) (a) Green, B. S.; Rabinsohn, Y.; Rejtö, M. *J. Chem. Soc., Chem. Commun.* **1975**, 313. (b) Tolbert, L. M.; Ali, M. B. *J. Am. Chem. Soc.* **1982**, *104*, 1742. (c) Haag, D.; Scharf, H.-D. *J. Org. Chem.* **1996**, *61*, 6127. (d) Saito, H.; Mori, T.; Wada, T.; Inoue, Y. *J. Am. Chem. Soc.* **2004**, *126*, 1900. (e) Saito, H.; Mori, T.; Wada, T.; Inoue, Y. *Chem. Commun.* **2004**, 1652. (f) Saito, H.; Mori, T.; Wada, T.; Inoue, Y. *Org. Lett.* **2006**, *8*, 1909.

(5) (a) Lange, G. L.; Decicco, C.; Tan, S. L.; Chamberlain, G. *Tetrahedron Lett.* **1985**, *26*, 4707. (b) Green, A. E.; Charbonnier, F. *Tetrahedron Lett.* **1985**, *26*, 5525. (c) Herzog, H.; Koch, H.; Scharf, H.-D.; Runsink, J. *Tetrahedron* **1986**, *42*, 3547. (d) Demuth, M.; Palomer, A.; Sluma, H.-D.; Dey, A. K.; Krüger, C.; Tsay, Y.-H. *Angew. Chem., Int. Ed. Engl.* **1986**, *25*, 1117. (e) Lange, G. L.; Decicco, C.; Lee, M. *Tetrahedron Lett.* **1987**, *28*, 2833. (f) Sato, M.; Takayama, K.; Furuya, T.; Inukai, N.; Kaneko, C. *Chem. Pharm. Bull.* **1987**, *35*, 3971. (g) Tsutsumi, K.; Yanagisawa, Y.; Furutani, A.; Morimoto, T.; Kakiuchi, K.; Wada, T.; Mori, T.; Inoue, Y. *Chem.—Eur. J.* **2010**, *16*, 7448.

(6) (a) Gotthardt, H.; Lenz, W. *Angew. Chem., Int. Ed. Engl.* **1979**, *18*, 868. (b) Jarosz, S.; Zamojski, A. *Tetrahedron* **1982**, *38*, 1447. (c) Koch, H.; Runsink, J.; Scharf, H.-D. *Tetrahedron Lett.* **1983**, *24*, 3217. (d) Nehrings, A.; Scharf, H.-D.; Runsink, J. *Angew. Chem., Int. Ed. Engl.* **1985**, *24*, 877. (e) Runsink, J.; Koch, H.; Nehrings, A.; Scharf, H.-D. *J. Chem. Soc., Perkin Trans. 2* **1988**, 49. (f) Buschmann, H.; Scharf, H.-D.; Hoffmann, N.; Plath, M. W.; Runsink, J. *J. Am. Chem. Soc.* **1989**, *111*, 5367. (g) Hegedus, L. S.; Bates, R. W.; Söderberg, B. C. *J. Am. Chem. Soc.* **1991**, *113*, 923. (h) Buschmann, H.; Hoffmann, N.; Scharf, H.-D. *Tetrahedron: Asymmetry* **1991**, *2*, 1429. (i) Matsumura, K.; Mori, T.; Inoue, Y. *J. Am. Chem. Soc.* **2009**, *131*, 17076. (j) Matsumura, K.; Mori, T.; Inoue, Y. *J. Org. Chem.* **2010**, *75*, 5461.

(7) (a) Fukuhara, G.; Nakamura, T.; Yang, C.; Mori, T.; Inoue, Y. *J. Org. Chem.* **2010**, *75*, 4307. (b) Fukuhara, G.; Nakamura, T.; Yang, C.; Mori, T.; Inoue, Y. *Org. Lett.* **2010**, *12*, 3510. (c) Yang, C.; Ke, C.; Liang, W.; Fukuhara, G.; Mori, T.; Liu, Y.; Inoue, Y. *J. Am. Chem. Soc.* **2011**, *133*, 13786.

(8) (a) Côté, G. L.; Biely, P. *Eur. J. Biochem.* **1994**, *226*, 641. (b) Bradbrook, G. M.; Gessler, K.; Côté, G. L.; Momany, F.; Biely, P.; Bordet, P.; Pérez, S.; Imberty, A. *Carbohydr. Res.* **2000**, *329*, 655. (c) Nishimoto, T.; Aga, H.; Mukai, K.; Hashimoto, T.; Watanabe, H.; Kubota, M.; Fukuda, S.; Kurimoto, M.; Tsujisaka, Y. *Biosci., Biotechnol., Biochem.* **2002**, *66*, 1806. (d) Dunlap, C. A.; Côté, G. L.; Momany, F. A. *Carbohydr. Res.* **2003**, *338*, 2367. (e) Furihata, K.; Fujimoto, T.; Tsutsui, A.; Machinami, T.; Tashiro, M. *Carbohydr. Res.* **2005**, *340*, 2060. (f) Furihata, K.; Fujimoto, T.; Tsutsui, A.; Machinami, T.; Tashiro, M. *Magn. Reson. Chem.* **2005**, *43*, 1044.

(9) Fukuhara, G.; Nakamura, T.; Kawanami, Y.; Yang, C.; Mori, T.; Hiramatsu, H.; Dan-oh, Y.; Tsujimoto, K.; Inoue, Y. *Chem. Commun.* **2012**, *48*, 9156. The rigidity of the CNN skeleton was given in this literature.

(10) Yang, C.; Mori, T.; Origane, Y.; Ko, Y. H.; Selvapalam, N.; Kim, K.; Inoue, Y. *J. Am. Chem. Soc.* **2008**, *130*, 8574.

(11) (a) Harada, N.; Nakanishi, K. In *Circular Dichroic Spectroscopy—Exciton Coupling in Organic Stereochemistry*; University Science Books: Mill Valley, CA, 1983. (b) Berova, N.; Bari, L. D.; Pescitelli, G. *Chem. Soc. Rev.* **2007**, *36*, 914.

(12) Wakai, A.; Fukasawa, H.; Yang, C.; Mori, T.; Inoue, Y. *J. Am. Chem. Soc.* **2012**, *134*, 4990. **2012**, *134*, 10306 (erratum).

(13) Dawn, A.; Shiraki, T.; Haraguchi, S.; Sato, H.; Sada, K.; Shinkai, S. *Chem.—Eur. J.* **2010**, *16*, 3676.